FULL PAPER

Solar events and solar wind conditions associated with intense geomagnetic storms

Shinichi Watari[1*] , Aoi Nakamizo[1] and Yusuke Ebihara[2]

Abstract

Intense magnetic storms pose a systemic threat to the electric power grid. In this study we examined the solar/ interplanetary causes of such storms, their peak theoretical and observed intensities, and their occurrence frequency. Using coronal mass ejection (CME) and solar wind data, we selected the 18 intense magnetic storms from 1996 to 2021 with disturbance storm time (Dst) index of less than − 200 nT and analyzed solar events and solar wind conditions associated with them. Approximately 83% of the CMEs associated with the storms were full halo type and more than 83% of the flares associated with the storms were located within 30 degrees in longitude of solar central meridian. The integrated dawn-to-dusk electric field in the solar wind (E_y) showed a good correlation with |min. Dst| of the storms and the peak E_y (E_{yp}) and the peak southward interplanetary magnetic field showed next good correlations with |min. Dst|. We obtained the E_{yp} of 236 mV/m for |min. Dst| of 2500 nT of the expected upper limit of Earth's magnetosphere using the empirical equations from the correlations between |min. Dst| and solar wind parameters and showed that this value of E_y is possible according to the past observations. The E_{yp} of 54 mV/m for the 13 March 1989 storm and that of 165/79 mV/m for the Carrington storm (|min. Dst|= 1760/850 nT) were also obtained. The analysis using the complimentary cumulative distribution function suggested the probabilities of E_y of 100, 200, 250, and 340 mV/m over the next 100 years to be 0.563, 0.110, 0.060 and 0.026, respectively.

Keywords Geomagnetic storm, Disturbance storm time (Dst) index, Ring current, Solar wind electric field, Coronal mass ejection (CME), Soft X-ray (SXR) flare, Complimentary cumulative distribution function (CCDF), Carrington storm, 13 March 1989 storm

Graphical Abstract
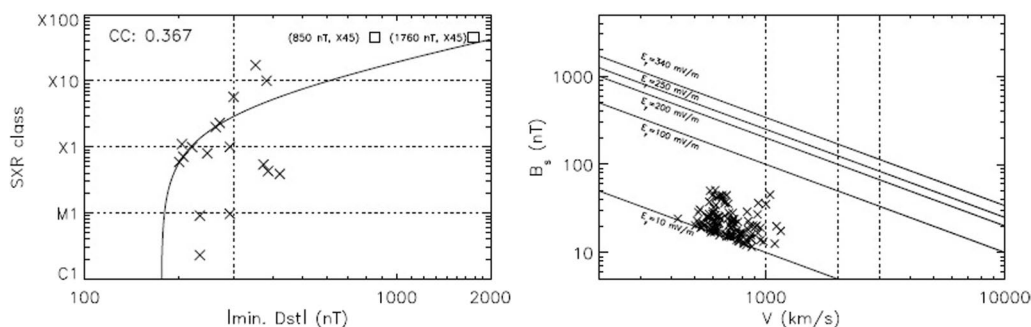
*Correspondence:
Shinichi Watari
watari@nict.go.jp
Full list of author information is available at the end of the article

Springer Open

Watari *et al. Earth, Planets and Space* (2023) 75:90

Page 2 of 15

Introduction

Studies of space weather hazards (Committee on the social and economic impacts of severe space weather events 2008; Cannon et al. 2013; Knipp et al. 2021) have revealed that severe space weather affects our social facilities. Intense geomagnetic storms are one of the space weather hazards. For example, geomagnetically induced current (GIC) by an intense geomagnetic storm on 13 March 1989 caused a power blackout in Quebec, Canada (Bolduc 2002; Boteler 2019).

To prepare for such a large geomagnetic storm, it is necessary to study the solar events and solar wind conditions associated with it. And it is useful for space weather forecasts to find a simple parameter suggesting occurrence of an intense storm. Several studies have been conducted on this. For example, Vennerstrom et al. (2016) and Lefevre et al. (2016) studied extreme geomagnetic storms between 1868 and 2010 using aa-index and the related activities with them. Zhang et al. (2007a, b), Meng et al. (2019), and Cliver et al. (2022) examined solar and interplanetary causes of the major storms considering Disturbance storm time (Dst) index of less than − 100, − 250, and − 300 nT, respectively. According to their results, major storms are associated with sheaths and magnetic clouds of interplanetary coronal mass ejections (ICMEs) originated from large active regions near center of the Sun.

On the solar wind condition, Gonzalez and Tsurutani (1987) analyzed ten storms with Dst < − 100 nT from August 1978 to December 1979 and showed that these storms were associated with the southward interplanetary magnetic field (IMF) > 10 nT with the dawn-to-dusk electric field in the solar wind (Ey) of more than 5 mV/m lasting for the time intervals of more than 3 h. Echer et al. (2008b) analyzed 90 storms with peak Dst (Dst_p) ≤ − 100 nT between 1996 and 2006. Following to the previous studies, we use Dst_p to refer the peak value of Dst in this section. They reported that Dst_p and the peak E_y (E_{yp}) have a high correlation coefficient (R) of − 0.86, and Dst_p and the peak of the southward IMF (B_s) show a slightly lower R of − 0.80. Gonzalez and Echer (2005) studied 64 storms with Dst ≤ − 85 nT and showed R of − 0.87 between Dst_p and E_{yp}, R of − 0.82 between Dst_p and the peak B_s (B_{sp}), and R of − 0.53 between Dst_p and the integrated E_y (E_{yi}) up to the time of the peak B_s. Contrary to these results, Echer et al. (2008a) showed R of −0.23 between Dst_p and E_{yp}, R of − 0.23 between Dst_p and B_{sp}, and R of − 0.62 between Dst_p and E_{yi} from the start of Dst decrease to the peak Dst for eleven storms with Dst_p ≤ − 250 nT.

The storm evolution is expressed by the Burton's equation (Burton et al. 1975; O'Brien and McPherron 2000),

$$\frac{dDst_0}{dt} = Q - \frac{Dst_0}{\tau} \qquad (1)$$

where Q is the injection rate, τ is the decay time constant, and Dst_0 is the corrected Dst on contribution of the magnetopause current. Burton et al. 1975 and O'Brien and McPherron 2000 considered that Q is proportional to E_y for southwards IMF. Hence, E_y is an important parameter to determine the storm evolution.

When $dDst_0/dt$ becomes zero in Eq. (1), Q_b is given by

$$Q\_b = Dst_{0\_b} / \tau, \qquad (2)$$

where Q_b is a value corresponding to Dst_{0_b}.

Equation (2) implies that the rate of energy input into the ring current is balanced with the rate of loss of energy stored in the ring current.

The injection rate Q is most likely related to the dawn-dusk magnetospheric convection electric field that transports hot ions in the plasma sheet on the nightside to the inner magnetosphere (Ebihara and Ejiri 2003). The magnitude of the magnetospheric convection can be approximated by the cross polar cap potential (CPCP). The CPCP is known to saturate under strong E_y condition (Reiff et al. 1981; Reiff and Luhmann 1986; Wimmer et al. 1990). On the other hand, Russell et al. (2001) were the first to suggest that the ring current is not affected by this saturation. Lopez et al. (2009) confirmed this using a simulation model. Myllys et al. (2016) analyzed geomagnetic storms with the symmetric disturbance field in H (SYM-H) index of less than – 50 nT and showed that SYM-H does not saturate to the solar wind electric field using OMNI data. Here, the one-minute SYM-H index (Iyemori 1990; Iyemori et al. 2010) is essentially the same as the hourly Dst index (Sugiura 1964).

For a possible large geomagnetic storm, there are studies based on statistical possibility analysis. Watari et al. (2001) reported the return periods of large Dst using the Weibull distribution. Figure 3 in Watari et al. (2001) suggested the return period of approximately 100 years for Dst of− 600 nT. Tsubouchi and Omura (2007) estimated an occurrence probability of Dst of− 589 nT corresponding to the March 1989 storm is approximately 1/60 y^{-1}. Riley (2012) obtained a probability of a storm with Dst of− 1700 nT of 0.015 for the next decade assuming a power law distribution. Love (2012) showed that the most likely Poisson occurrence probability for another Carrington-type event in the next 10 years is 0.063. Kataoka (2013) estimated that the probability of another Carrington-type storm occurring over the next decade is 0.04−0.06. Theoretically, Vasyliunas (2010) obtained the upper limit of |min. Dst| of 2500 nT based on the Dessler−Parker−Sckopke theorem.

Watari *et al. Earth, Planets and Space*   (2023) 75:90

Page 3 of 15

Major causes of geomagnetic storms are ICMEs and corotating interaction regions (CIRs) associated with high-speed solar wind stream from coronal holes (Tsurutani and Gonzalez 1997, and references therein). Richardson et al. (2006) showed that maximum CIR-storm strength is Dst of − 180 nT. Hence, storms with Dst of less than – 200 nT are considered to be mainly caused by ICMEs.

Continuous observations of coronal mass ejections (CMEs) and solar wind by space assets began in the 1990s. We studied solar events and solar wind conditions associated with intense geomagnetic storms with |min. Dst| of more than 200 nT between 1996 and 2021 in order to examine E_{yp} corresponding to the upper limit of Dst using the relationship between |min. Dst| and the E_{yp} and a possibility of such a value of E_y. |min. Dst| is equal to the absolute value of peak Dst (Dst_p) of the storms. The final Dst up to 2016 was used in our analysis while the preliminary or real-time Dst (World Data Center (WDC) for Geomagnetism, Kyoto 2022) were often used in the previous studies. The intense storms with Dst of less than− 200 nT have been not observed after 2016 because of low solar activity.

We also estimated the E_{yp} of the 13 March 1989 storm (Bolduc 2002; Boteler 2019) and the 1859 Carrington storm (Carrington 1859; Tsurutani et al. 2003; Cliver and Svalgaard 2004; Siscoe et al. 2006) and the occurrence probability of E_y corresponding to the upper limit of Dst using the complimentary cumulative distribution function (CCDF).

Data and analysis

Observations of CMEs and solar wind have been conducted almost continuously after 1996. Hence, we used the data obtained by such observations between 1996 and 2021 for our analysis. We selected storms with Dst < − 200 nT to pick-up storms mainly associated with ICMEs (Richardson et al. 2006). Eighteen geomagnetic storms were selected during this period, on the basis of the report of geomagnetic storms from the Kakioka Magnetic Observatory (2015). The Dst index was obtained from the World Data Center for Geomagnetism, Kyoto (2015) and the final Dst was available up to 2016 on this analysis. Solar events associated with the geomagnetic storms were investigated using the SOHO LASCO CME catalog (https://cdaw.gsfc.nasa.gov/CME_list/index.html) and the Geostationary Operational Environment Satellites (GOES) flare reports archived in the National Centers for Environmental Information (NCEI), NOAA (https://ngdc.noaa.gov/ngdc.html). Solar wind conditions in the geocentric solar magnetic (GSM) coordinates were analyzed using the hourly averaged OMNI data (https://spdf.gsfc.nasa.gov/pub/data/omni/low_res_

omni/). In the OMNI data, the time tag shows the first hour of the average and the same time tag is used for Dst index.

Eruptive flares and CMEs associated with the storms were investigated using expected occurrence time at the Sun calculated by the in situ solar wind speed. The GOES flare reports and extreme ultra-violet (EUV) images linked from the SOHO LASCO CME catalog were also used to identify the eruptive flares associated with the CMEs.

Table 1 shows a list of the geomagnetic storms (|min. Dst|> 200 nT) along with the solar events and solar wind conditions. The selected storms consist of 16 storms with sudden commencements (SSCs) and two storms with gradual commencements (SGs). Table 1 shows the peak values, selected in the period before |min. Dst|, of speed (V): V_p, B_s: B_{sp}, and total magnetic field (B): B_p, and E_y: E_{yp} with their maximum time and the integrated E_y (E_{yi}). The E_{yi} was calculated according to Echer et al. (2008a).

Figure 1 shows histograms of time differences between |min. Dst| and B_p, B_{sp}, V_p, and E_{yp}, respectively. The average time differences between |min. Dst| and B_p, B_{sp}, V_p, and E_{yp} was 4.7 ± 3.7 h, 3.3 ± 2.2 h, 4.4 ± 4.7 h, and 3.3 ± 2.1 h, respectively. Approximately 90% of the B_{sp} and the E_{yp} occurred within 5 h before |min. Dst|.

Table 1 also showed eruptive flares and CMEs associated with the storms. In Table 1, a CME with an apparent width of 360 deg. is called 'a full halo CME' by a coronagraph observation to contrast it with 'a partial halo CME'. For the gaps in the OMNI plasma data, we calculated hourly values of V using the speed of alpha particles observed by the Solar Wind Ion Composition Spectrometer (SWICS) of the Advanced Composition Explorer (ACE) spacecraft (https://spdf.gsfc.nasa.gov/pub/data/ace/swics/). According to Steiger et al. (2000), the speed of solar wind alpha particles generally agrees with the speed of solar wind protons within 0.5%. The hourly values of E_y were calculated using the speeds by the SWICS and the OMNI magnetic field data.

For estimation of the correlation analysis, we showed *T* and p-value, an occurrence probability of *T*.

$$T = \frac{R}{\sqrt{1 - R^2}} \sqrt{N - 2}, \tag{3}$$

where *N* is number of data points and *R* is a correlation coefficient. A value of *T* follows t-distribution with *N–2* degrees of freedom (Kurihara 2001)

For estimation of the fitting by

$$y = a + bx, \tag{4}$$

where *a* and *b* are constants, we showed *F* and p-value, an occurrence probability of *F*.

Table 1 Geomagnetic storms with Dst of less than − 200 nT between 1996 and 2021 and solar events and solar wind conditions associated with them

| No	Magnetic storm[a1]		type	|min. Dst| (nT)	Peak V (V_p) (km/s)	Peak B_s (B_{sp}) (nT)	Peak B (B_p) (nT)	Peak E_y (E_{yp}) (mVm^{-1})	Integrated E_y (E_{yi}) (mVm^{-1} h)	Solar event	
	Start	End								Flare	CME
1	1998/05/03 1743 UT	1998/05/05 2100 UT	SSC	05/04 05 UT 205	05/04 04 UT 834	05/04 04 UT 29.0	05/04 04 UT 39.1	05/04 04 UT 24.19	59.94	05/02 1331 UT X1.1/3B (S15W15)	05/02 1406 UT full halo (938 km/s)
2	1998/09/24 2345 UT	1998/09/26 0000 UT	SSC	09/25 09 UT 207	09/25 07 UT 820	09/25 02 UT 17.8	09/25 00 UT 28.6	09/25 02 UT 13.44	62.04	09/23 0640 UT M7.1/3B (N18E09)	N/A
3	1999/10/21 1554 UT	1999/10/23 1000 UT	SG	10/22 06 UT 237	10/22 06 UT 548	10/22 05 UT 30.7	10/22 05 UT 35.8	10/22 05 UT 16.24	70.59	No obvious corresponding flare	10/18 0006 UT partial halo (AW = 240 deg.) (144 km/s)
4	2000/04/06 1639 UT	2000/04/07 2000 UT	SSC	04/07 00 UT 292	04/06 18 UT 590	04/06 21 UT 27.3	04/06 22 UT 31.4	04/06 21 UT 15.78	102.82	04/04 1511 UT C9.7/2F (N16W66)	04/04 1632 UT full halo (1188 km/s)
5	2000/07/15 1436 UT	2000/07/16 1800 UT	SSC	07/16 00 UT 300	07/15 21 UT 1107	07/15 20 UT 45.3	07/15 20 UT 51.6	07/15 20 UT 47.11	130.78	07/14 1003 UT X5.7/3B (N22W07)	07/14 1054 UT full halo (1674 km/s)
6	2000/08/11 1846 UT	2000/08/13 1600 UT	SSC	08/12 09 UT 234	08/12 04 UT 672	08/12 08 UT 28.7	08/12 09 UT 33.6	08/12 08 UT 17.33	83.44	08/09 1533 UT C2.3/SF (N11W11)	08/09 1630 UT full halo (702 km/s)
7	2000/09/17 1424 UT	2000/09/19 0000 UT	SG	09/17 23 UT 201	09/17 23 UT 795	09/17 21 UT 23.9	09/17 18 UT 30.0	09/17 21 UT 14.94	32.41	09/16 0406 UT M5.9/2B (N14W07)	09/16 0518 UT full halo (1215 km/s)
8	2001/03/31 0052 UT	2001/04/01 1500 UT	SSC	03/31 08 UT 387	03/31 04 UT 716*2	03/31 06 UT 44.7*2	03/31 01 UT 48.2*2	03/31 06 UT 30.62*2	90.08	03/28 1121 UT*2 M4.3/SF (N18E02)*2	03/28 1250 UT*2 full halo (519 km/s)*2
9	2001/04/11 1343 UT	2001/04/12 1900 UT	SSC	04/11 23 UT 271	04/11 20 UT 732	04/11 23 UT 20.5	04/11 23 UT 34.5	04/11 23 UT 14.86	64.08	04/10 0506 UT X2.3/3B (S23W09)	04/10 0530 UT full halo (2411 km/s)
10	2001/11/06 0151 UT	2001/11/07 2000 UT	SSC	11/06 06 UT 292	11/06 06 UT 789*3	11/06 02 UT 57.8	11/06 02 UT 62.0	11/06 02 UT 44.06*3	97.39	11/04 1603 UT X1.0/3B (N06W18)	11/04 1635 UT full halo (1810 km/s)
11	2001/11/24 0555 UT	2001/11/26 0000 UT	SSC	11/24 16 UT 221	11/24 14 UT 1040	11/24 11 UT 22.7	11/24 09 UT 50.1	11/24 11 UT 19.14	58.16	11/22 2232 UT M9.9/2N (S15W34)	11/22 2330 UT full halo (1437 km/s)

Table 1 (continued)

| No | Magnetic storm[a1] | | | |min. Dst| (nT) | Peak V (V_p) (km/s) | Peak B_s (B_{sp}) (nT) | Peak B (B_p) (nT) | Peak E_y (E_{yp}) (mVm^{-1}) | Integrated E_y (E_{yi}) (mVm^{-1} h) | Solar event | | CME |
	Start	End	type								Flare		
12	2003/10/29 0611 UT	C	SSC	10/30 00 UT 353	10/29 08 UT 1917*3	10/29 19 UT 26.5	10/29 16 UT 47.3	10/29 19 UT 29.36*3	146.79		10/28 0951 UT X17.2/4B (S16E08)	10/28 1130 UT full halo (2459 km/s)
13	2003/10/30 1637 UT	2003/11/02 2100 UT	SSC	10/30 22 UT 383	10/30 18 UT 1891*3	10/30 20 UT 27.1	10/30 19 UT 38.0	10/30 19 UT 44.03*3	139.14		10/29 2037 UT X10.0/2B (S15W02)	10/29 2054 UT full halo (2029 km/s)
14	2003/11/20 0802 UT	2003/11/22 0000 UT	SSC	11/20 20 UT 422	11/20 11 UT 703	11/20 15 UT 50.9	11/20 15 UT 55.8	11/20 15 UT 31.25	190.50		11/18 0812 UT M3.9 (S02E18)	11/18 0850 UT full halo (1660 km/s)
15	2004/11/07 1827 UT	C	SSC	11/08 06 UT 374	11/08 06 UT 728	11/08 03 UT 44.9	11/07 23 UT 47.8	11/08 03 UT 29.5	207.81		11/04 2253 UT M5.4 (N08E18)	11/04 2330 UT partial halo (AW > 293 deg) (1055 km/s)
16	2004/11/09 1849 UT	2004/11/13 0000 UT	SSC	11/10 10 UT 263	11/09 22 UT 824	11/10 06 UT 24.0	11/09 21 UT 40.3	11/10 06 UT 17.69	101.23		11/07 1542 UT X2.0 (N09W17)	11/07 1654 UT full halo (1759 km/s)
17	2005/05/16 0238 UT	2005/05/16 1800 UT	SSC	05/15 08 UT 247	05/15 06 UT 928	05/15 06 UT 36.5	05/15 08 UT 54.8	05/15 06 UT 33.87	68.38		05/13 1613 UT M8.0/2B (N12E12)	05/13 1712 UT full halo (1689 km/s)
18	2015/03/17 0445 UT	2015/03/21 1500 UT	SSC	03/17 22 UT 234	03/17 11 UT 614	03/17 14 UT 18.6	03/17 14 UT 31.5	03/17 14 UT 10.55	94.01		03/15 0115 UT C9.1/1F (S22W25)	03/15 0148 UT full halo (719 km/s)

SSC storm with a sudden commencement, *SG* storm with a gradual commencement, *C* continue, *N/A* not available, *AW* angular width

[a] 1: based on the report of Kakioka magnetic observatory

[b] 2: corresponding to the first ICME

[c] 3: based on speed of alpha particles observed by the ACE/SWICS
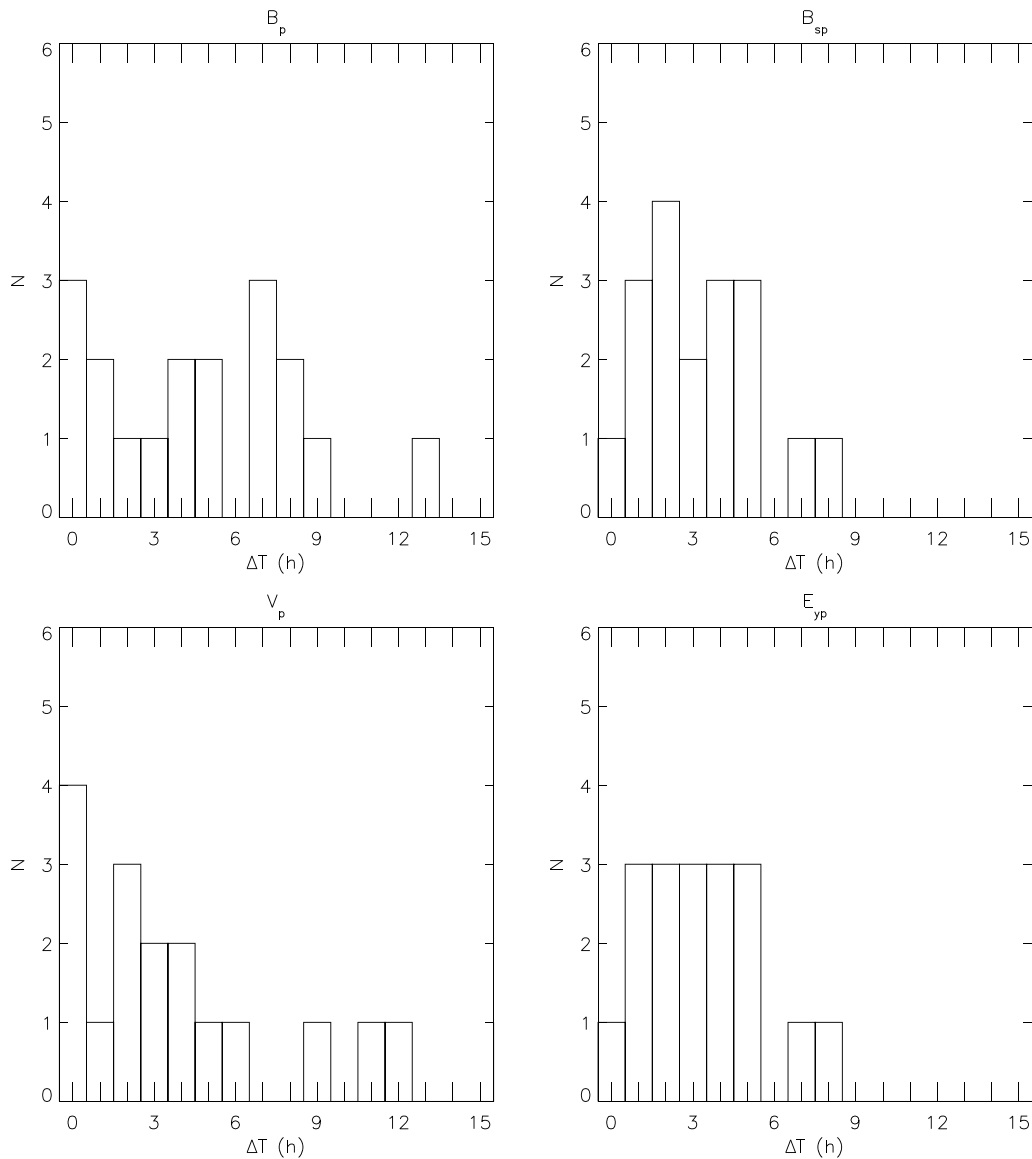
Fig. 1 Histograms of the time differences between |min. Dst| and B_p, B_{sp}, V_p, and E_{yp}

$$F = \frac{V_R}{V_e}, \tag{5}$$

where

$$V_R = \sum_{i=1}^{N} ((a + bx_i) - \bar{y})^2, \tag{6}$$

$$V_e = \frac{1}{N-2} \sum_{i=1}^{N} (y_i - (a + bx_i))^2, \tag{7}$$

and

$$\bar{y} = \frac{1}{N} \sum_{i=1}^{N} y_i \tag{8}$$
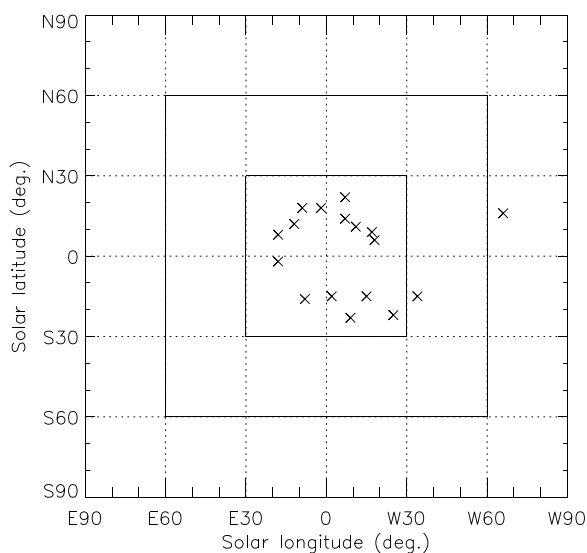
for x_i in x and y_i in y.

A value of F follows F-distribution with one degree of freedom in the numerator and N–2 degrees of freedom in the denominator (Kurihara 2001).

In this study, the p-values of less than 0.05 were considered that the obtained correlation coefficient or fitting is statistically significant.
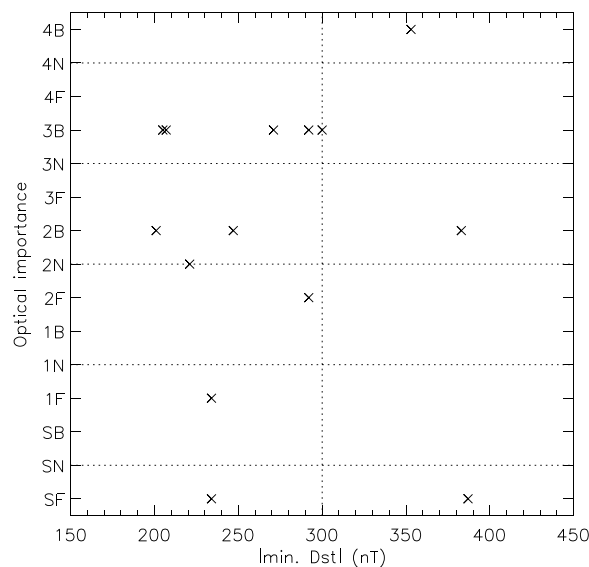
Watari *et al. Earth, Planets and Space*   (2023) 75:90

Page 7 of 15

Solar events associated with storms

According to Table 1, over 83% of the selected storms were associated with full halo CMEs. Figure 2 shows locations of the solar flares associated with the storms. More than 83% of the flares associated with the storms occurred within the solar longitude of 30 degrees, except for three storms. This suggests that a full halo CME originated near the solar center has a good chance of hitting Earth with its main body and producing intense geomagnetic storms. No obvious corresponding flare was found for the no. 3 event. For the no. 4 event, the dimming channel expanded toward the southeast direction, according to the SOHO/Extreme ultraviolet Imaging Telescope (EIT) data linked from the SOHO LASCO CME catalog. The no. 11 event occurred in the bright and wide area around W34 degrees, according to the EIT data.

Figure 3 shows a scatter plot of |min. Dst| of the storms and optical importance of the flares associated with the storms. The optical importance is determined by the area (S: ≤ 2.0 hemisphere square degrees, 1: $2.1-5.1$ square degrees, 2: $5.2-2.4$ square degrees, 3: $12.5-24.7$ square degrees, and 4: ≥ 24.8 square degrees) and brilliance (F: faint, N: normal, and B: bright) of flares observed by ground-based H-alpha observations. Figure 4 shows a scatter plot of |min. Dst| of the storms and soft X-ray (SXR) class (A: $< 10^{-5}$ Wm^{-2}, B: $10^{-5}-10^{-6}$ Wm^{-2}, C: $10^{-6}-10^{-5}$ Wm^{-2}, M: $10^{-5}-10^{-4}$ Wm^{-2}, X: $> 10^{-4}$ Wm^{-2}) of the flares in association with the storms. The storm sizes expressed by |min. Dst| appear to be roughly proportional to the optical importance and SXR class of the flares. Three events in Table 1 (Nos. 8, 14, and 15) with Dst ≤ -300 nT were associated with
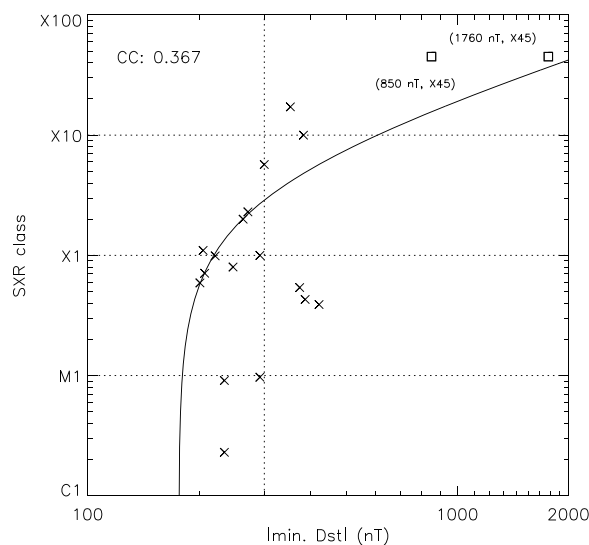

Fig. 3 A scatter plot of |min. Dst| and the optical importance of the flares associated with the intense geomagnetic storms

M-class SXR flares. And the event No. 8 had an association with the SF optical flare according to the NOAA/GOES flare reports with the optical flare importance from ground-based observations. Zhang et al. (2007a, b) associated this event with the X1.7/SF flare.

The solid line in Fig. 4 shows the least squares (LS) fitting. Two square marks show the values of the Carrington event (|min. Dst|=1760/850 nT and SXR flare

Fig. 2 Locations of solar flares associated with the intense geomagnetic storms

Fig. 4 A scatter plot of |min. Dst| and the SXR class of the flares associated with the intense geomagnetic storms. Solid line shows the LS fitting. Square marks show the values of the 1859 Carrington event

Watari *et al. Earth, Planets and Space*   (2023) 75:90

Page 8 of 15
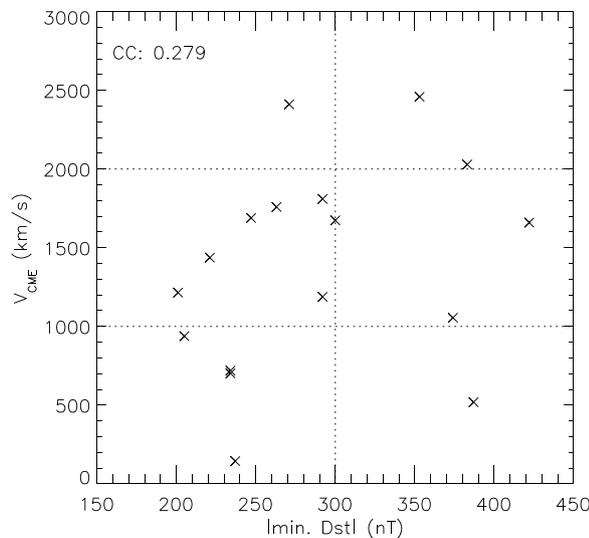
Fig. 5 A scatter plot of |min. Dst| and CME speed (V_{CME}) associated with the intense geomagnetic storms

Table 2 R, T, and p-values of |min. Dst| vs. SXR class and |min. Dst| vs. CME speed

Parameter	R	T	p-value
|min. Dst| vs. SXR class	0.367	1.528	0.147
|min. Dst| vs. CME speed	0.279	1.125	0.278

class of X45) reported by Tsurutani et al. (2003), Siscoe et al. (2006), and Cliver and Dietrich (2013).

Figure 5 shows a scatter plot of |min. Dst| and CME speed. Here, we used the linear speeds taken from the SOHO LASCO CME catalog. The storms with |min. Dst| of more than 300 nT are associated with the CMEs with speed of more than 1000 km/s, except for the no. 8 storm. The no. 8 storm was associated with two interplanetary CMEs (ICMEs). The second fast CME caught up to the first one on the way to Earth (Farrugia and Berdichevsky 2004). Table 2 shows T and p-values for R of |min. Dst| vs. SXR class and |min. Dst| vs. CME speed. The CME speeds show a weak positive correlation with |min. Dst|. This could be because the CME speeds are apparent speeds containing a projection effect.

Solar wind conditions associated with storms
Figure 6 shows scatter plots of |min. Dst| of the storms and the solar wind parameters at 1 AU shown in Table 1: B_p, B_{sp}, V_p, E_{yp}, E_{yi}, and integration time of E_y. Table 3 shows R, T, and p-values of |min. Dst| and solar wind parameters shown in Fig. 6. The p-values were less than 0.05 except for R of |min. Dst| vs. V_p and |min. Dst| vs. integration time of E_y. The E_{yi} showed a good correlation

with |min. Dst| (R of 0.838) as reported by Echer et al. (2008a). However, the integration time of E_y varied from storm to storm in the range of 3–12 h and R of |min. Dst| vs. the integration time of E_y (R of 0.121) was small. The average of the integration time of E_y was 7.7 ± 2.7 h. The E_{yp} (R of 0.586) and the B_{sp} (R of 0.579) showed the next good correlations as reported by Gonzalez and Echer (2005), Echer et al. (2008a), Echer et al. (2008b), Echer et al. (2013), and Rawat et al. (2018).

We obtained the empirical equations using the LS fitting for |*min. Dst*| vs. E_{yi}, |*min. Dst*| vs. B_{sp}, and |*min. Dst*| vs. E_{yp}, respectively.

$$E_{yi} = 0.556 \times |min.Dst| - 58.238 \, \text{mV/m-h} \tag{9}$$

$$E_{yp} = 0.095 \times |min.Dst| - 1.912 \, \text{mV/m} \tag{10}$$

$$B_{sp} = 0.097 \times |min.Dst| + 4.465 \, \text{nT} \tag{11}$$

Table 4 shows F and p-values for the fitting of the above three equations. The p-values of the three equations were less than 0.05.

|min. Dst| (=589 nT) of the 13 March 1989 storm is the largest one since 1957. However, successive solar wind data during the main phase of the storm are unavailable. The E_{yi} of 269 mV/m-h, E_{yp} of 54 mV/m, and B_{sp} of 62 nT were obtained using Eqs. (9), (10), and (11).

According to Boteler (2019), this storm was caused by two CMEs: the first associated with a X4.5 flare on 10 March and the second linked to a M7.3 flare on 12 March.

A sudden impulse (SI) caused by the second CME and the substorm triggered by this SI impacted the Hydro-Quebec system. For the second CME, Boteler (2019) calculated the maximum solar wind speed of 983 km/s at 1 AU from the average shock transit speed of 1320 km/s using Cliver et al.'s empirical Eq. (1990); the relationship between the average shock transit speed ($V_{\_tr}$) from the Sun to Earth and the maximum solar wind speed at Earth ($V_{\_max}$) is given by

$$V_{\_max} = 0.775 V_{\_tr} - 40 \, \text{km/s} \tag{12}$$

For E_{yp} of 54 mV/m and $V_{\_max}$ of 983 km/s, we calculated the expected B_s (= $E_{yp}/V_{\_max}$) to be 55 nT. This value is consistent with the B_s range of 40–60 nT suggested by Boteler (2019).

For the Carrington storm that occurred 17.5 h after the white light flare (Carrington 1859), |min. Dst| is estimated to be 1760 nT (Tsurutani et al. 2003), or 850 nT (Siscoe et al. 2006). Using Eqs. (9), (10), and (11), we obtained E_{yi} of 920 mV/m-h, E_{yp} of 165 mV, and B_{sp} of 175 nT for |min. Dst| of 1760 nT and E_{yi} of 414 mV/m-h, E_{yp} of 79 mV, and B_{sp} of 87 nT for |min. Dst| of 850 nT.
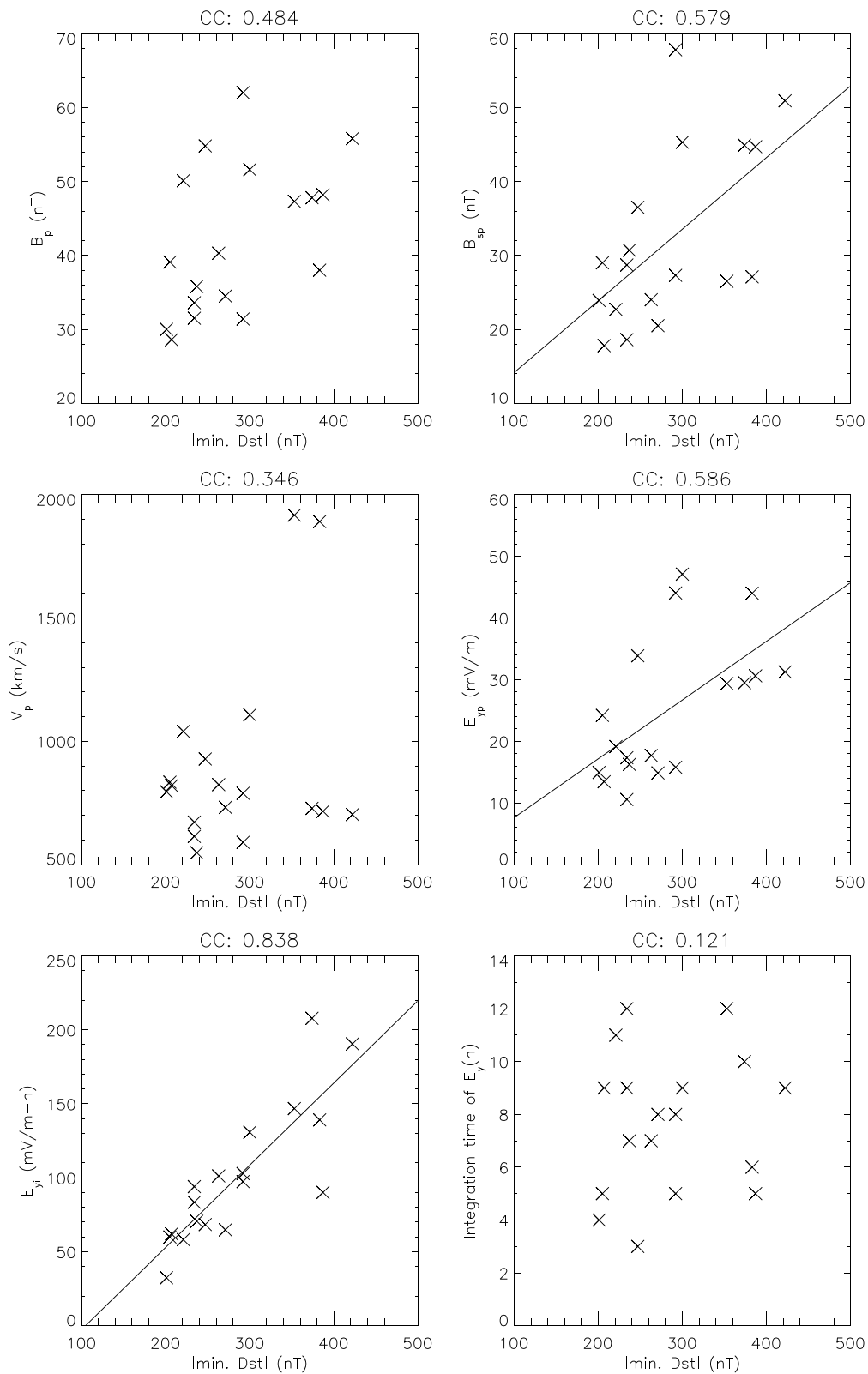
Fig. 6 Scatter plots of |min. Dst| and solar wind parameters: B_p, B_{sp}, V_p, E_{yp}, E_{yi}, and integration time of E_y. Solid line shows the LS fittings of |min. Dst| vs. B_{sp}, |min. Dst| vs. E_{yp}, and |min. Dst| vs. E_{yi}, respectively

Table 3 R, T, and p-values of |min. Dst| and solar wind parameters

Parameter	R	T	p-value
|min. Dst| vs. Peak B (B$_p$)	0.484	2.212	0.0418
|min. Dst| vs. Peak Bs (B$_{sp}$)	0.579	2.841	0.0118
|min. Dst| vs. Peak V (V$_p$)	0.346	1.475	0.1596
|min. Dst| vs, Peak E$_y$ (E$_{yp}$)	0.586	2.893	0.0106
|min. Dst| vs. Integrated E$_y$ (E$_{yi}$)	0.838	6.143	0.00001
|min. Dst| vs. Integration time of E$_y$	0.121	0.488	0.6325

Table 4 F and p-values for the LM fittings of Eqs. (9), (10), and (11)

	F	p-value
Equation (9) for integrated E$_y$ (E$_{yi}$)	37.762	0.00001
Equation (10) for peak E$_y$ (E$_{yp}$)	8.309	0.0108
Equation (11) for peak B$_s$ (B$_{sp}$)	8.090	0.0117

V$_{\_max}$ of 1801 km/s is calculated applying the Eq. (12) to V$_{\_tr}$ of 2375 km/s (the travel time of 17.5 h). Recently Hayakawa et al. (2022) found that the transit time was shorter than previously considered ($\leq$17.1 h). V$_{_max}$ of 1843 km/s was obtained applying Eq. (12) to V$_{\_tr}$ of 2430 km/s corresponding to the travel time of 17.1 h.

Table 5 summarizes the estimated solar wind parameters of the Carrington storm. The values shown in Table 5 are consistent with that estimated by Tsurutani et al. (2003), who used an empirical relationship between the solar wind speed and peak magnetic field of ICMEs (Gonzalez et al. 1998).

Vasyliunas (2010) suggested that the upper limit of |min. Dst| is approximately 2500 nT based on the Dessler−Parker−Sckopke theorem. For |min. Dst| of

2500 nT, E$_{yi}$ of 1332 mV/m-h, E$_{yp}$ of 236 mV/m, and B$_{sp}$ of 247 nT were obtained using Eqs. (9), (10), and (11).

On the other hand, Tsurutani and Lakhina (2014) noted that the expected maximum solar wind electric field would be approximately 340 mV/m on the basis of an observed maximum CME speed of 3000 km/s near the Sun measured using the SOHO coronagraph data.

Figure 7 shows the relationship of B$_s$ and V for constant E$_y$ of 10, 100, 200, 250, and 340 mV/m with B$_s$ and V pairs for E$_y$ of more than 10 mV/m between 1996 and 2021 in the hourly averaged OMNI data. Cliver et al. (1990) reported the highest solar wind speed of 2170 km/s using V$_{\_tr}$ of 2850 km/s and Eq. (12) for the 4 August 1972 sudden commencement (SC). For this SC on 4 August 1972, Araki et al. (2004) estimated the interplanetary shock speed of 3080 km/s using the rise time of this SC. However, the storm associated with this SC was only |min. Dst| of 125 nT because the interplanetary magnetic field did not direct southward (Knipp et al. 2018). Araki (2014) analyzed the SCs between 1968 and 2013 and reported a shock speed over 2000 km/s for the 24 March 1940 SC, determined using the measured amplitude of the SC. STEREO A spacecraft (~1AU) measured solar wind speed of 2246 km/s associated with the shock of the 23 July 2012 CME, which missed Earth (Baker et al. 2013; Russell et al. 2013; Liu et al. 2014). This shock took only 18.6 h to reach STEREO A at 1 AU. The maximum IMF strength of 109 nT was observed associated with this event.

From these events, it is considered that a solar wind speed exceeding 2000 km/s is possible. If we assume V of 2000 km/s, B$_s$ of about 118 nT is necessary for |min. Dst| of 2500 nT, according to Fig. 7. For V of 3000 km/s, B$_s$ of 79 nT is necessary. These values are feasible on the basis of the above consideration.

Table 5 The V$_{\_tr}$, V$_{\_max}$, E$_{yi}$, E$_{yp}$, B$_s$, and B$_{sp}$ estimated using |min. Dst| of 1760 and 850 nT and transit time of 17.5 and 17.1 h on the Carrington storm

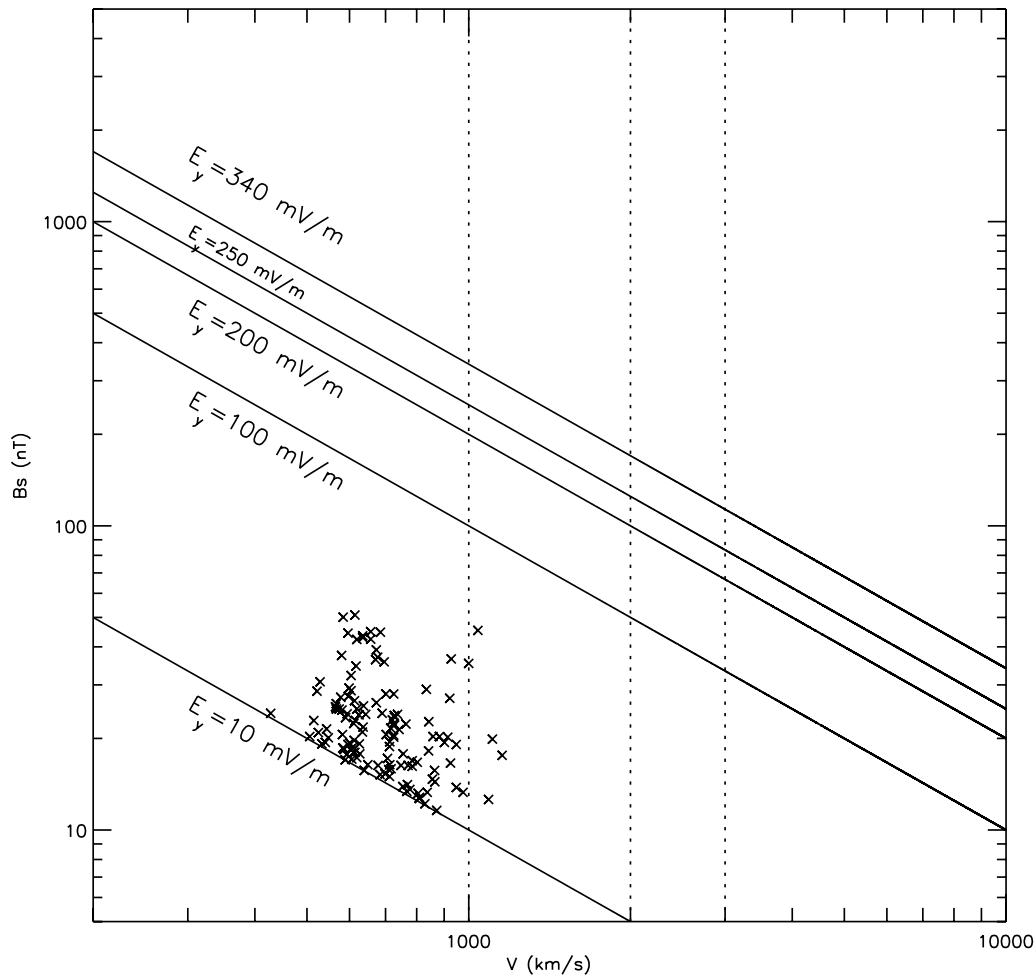| |min. Dst| (nT)	Transit time (h)	V$_{\_tr}$ (km/s)	V$_{\_max}$[1] (km/s)	Integrated E$_y$ (E$_{yi}$)[b2] (mV/m-h)	Peak E$_y$ (E$_{yp}$)[c3] (mV/m)	B$_s$[d4] (nT)	Peak B$_s$ (B$_{sp}$)[e5] (nT)
1760	17.1	2430	1843	920	165	90	175
1760	17.5	2375	1801	920	165	92	175
850	17.1	2430	1843	414	79	43	87
850	17.5	2375	1801	414	79	44	87

[a] 1: calculation by Eq. (12)

[b] 2: calculation by Eq. (9)

[c] 3: calculation by Eq. (10)

[d] 4: calculation by Eq. (10) and V$_{\_max}$

[e] 5: calculation by Eq. (11)

Fig. 7 Relationship of V and B_s for constant E_y of 10, 100, 250, and 340 mV/m and V and B_s pairs with E_y of more than 10 mV/m in the hourly averaged OMNI data between 1996 and 2021

Statistical analysis of extreme solar wind conditions

We estimated the probabilities of occurrence of large B, B_s, V, E_y, N, and P_d by applying Riley's statistical method (2012) to the hourly averaged OMNI data between 1996 and 2021. When the probability *p(x)* follows the power law, the cumulative distribution function *P(x)*, which expresses the probability of an event of magnitude equal to or greater than the critical value x_{crit}, also follows a power law.

$$p(x \geq x_{crit}) = \int_x^{\infty} p(x')\, dx' = \frac{C}{\alpha - 1} x^{-\alpha+1} \qquad (13)$$

The slope α and constant C are calculated as,

$$\alpha - 1 = N_p \left[\sum_{i=1}^{N_p} \ln \left(\frac{x_i}{x_{\_\min}} \right) \right]^{-1} \qquad (14)$$

and

$$C = \frac{\alpha - 1}{x_{\_\min}^{-\alpha+1}}, \qquad (15)$$

where x_i is the measured value of x, N_p is the total number of events for $x \geq x_{\_min}$, and $x_{\_min}$ is some appropriate minimum value of x below the breakdown of the power-law relationship.

The probability of one or more events greater than x_{crit} occurring during a certain time period Δt is

$$p(x \geq x_{crit}, t = \Delta t) = 1 - e^{-N_p \frac{\Delta t}{\tau} p(x \geq x_{crit})}, \qquad (16)$$

where τ is the total time span of the data set.

Figure 8 shows the CCDFs of B, B_s, V, E_y, N, and P_d for the 26-year OMNI data between 1996 and 2021. The observation data of B, B_s, V, E_y, N, and P_d cover 99.8%,

Watari *et al. Earth, Planets and Space* (2023) 75:90

Page 12 of 15

99.8%, 99.7%, 99.7%, 97.6%, and 97.6% of the 26 year period, respectively. Skoug et al. ([2004](#)) reported the highest directly measured solar wind speed of over 1850 km/s during the 29−30 October 2003 event. For this event, Zurbuchen et al. ([2004](#)) reported the speed of alpha particles of over 1900 km/s referring to the

ACE/SWICS data. Unfortunately, there is a gap in the OMNI data of the plasma measurement between 28 October 2003 and 3 November 2003 because of the presence of intense solar energetic particles.

We fitted a power law to the CCDFs above B_{min} of 30 nT, B_{s_min} of 20 nT, V_{min} of 800 km/s, E_{y_min} of 12 mV/m,
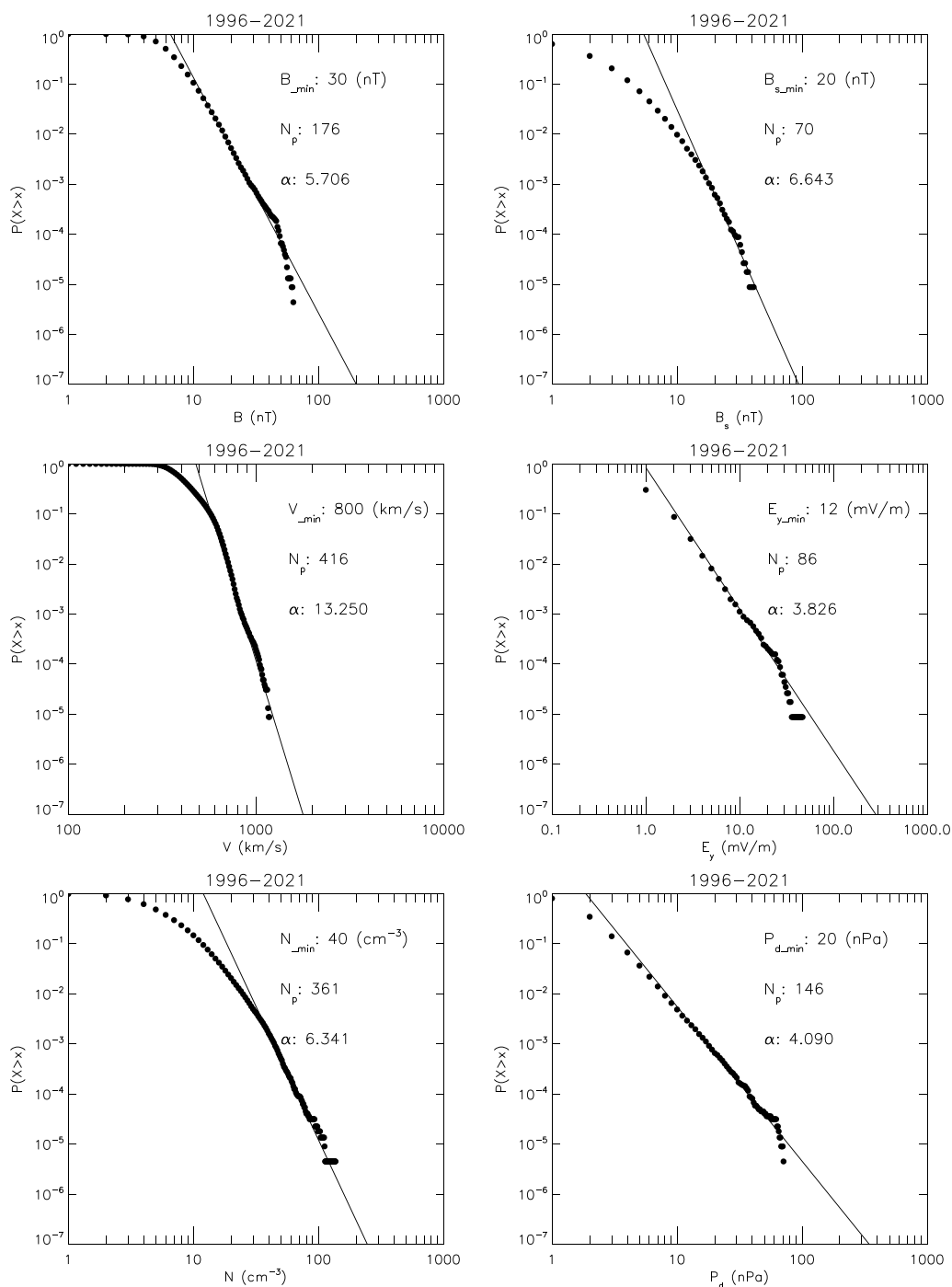
Fig. 8 CCDFs of B, B_s, V, E_y, N, and P_d for the hourly averaged OMNI data between 1996 and 2021. Solid lines show power law fittings

$N_{\_min}$ of 40 cm^{-3}, and P_{d_min} of 20 nPa in Fig. 8. The power law fittings in Fig. 8 are almost good. Deviations in the fittings of B, E_y, and P_d are only last 5 out of 176, 3 out of 86, and 2 out of 146 data, respectively. We obtained the occurrence probabilities of 0.904 for B = 100 nT, 0.030 for B_s = 100 nT, 0.021 for V = 2000 km/s, 0.060 for E_y = 250 mV/m, 0.226 for N = 200 cm^{-3}, and 0.027 for P_d = 500 nPa over the for 100 years using Eq. (16).

The occurrence probability of B_s is rather small compared to that of B because the probability that IMF will turn completely to the south is very low. The occurrence probabilities of E_y of 100, 200, 250, and 340 mV/m over the next 100 years are 0.563, 0.110, 0.060, and 0.026, respectively. Here, E_y of 100 and 200 mV/m correspond to |min. Dst| of 1073 and 2125 nT according to Eq. (10).

Riley (2012) reported that the possibility of |min. Dst| of 1700 nT (e.g., the 1859 Carrington storm) occurring over the next 10 years is 0.015. Love (2012) gave the probability of another Carrington-type storm in the next decade as 0.063 and Kataoka (2013) as 0.04–0.06. We obtained the occurrence probability of 0.020 for |min. Dst| of 1760 nT using the CCDF of E_y and Eq. (10). Our result is between their results.

Summary

We selected 18 magnetic storms with |min. Dst| of more than 200 nT using the final Dst and studied the solar events and solar wind conditions associated with them. We obtained the following results.

1. Over 83% of the storms were associated with full halo CMEs.
2. More than 83% of the flares associated with the storms were within 30 degrees solar longitude.
3. |min. Dst| and the E_{yi} showed a good correlation (R of 0.838) as shown by Echer et al. (2008a) while the integration time of E_y varied from storm to storm. The E_{yp} (R of 586) and the B_{sp} (R of 0.579) showed next good correlations with |min. Dst| as reported by Gonzalez and Echer (2005), Echer et al. (2008a), Echer et al. (2008b), Echer et al. (2013), and Rawat et al. (2018). We obtained the empirical equations based on these correlations and calculated the expected E_{yi}, E_{yp}, and B_{sp} of the March 1989 storm, the Carrington storm, and the expected upper limit of |min. Dst|, respectively.
4. We obtained the E_{yi} of 1332 mV/m-h, the E_{yp} of 236 mV/m, and the B_{sp} of 247 nT corresponding to the expected upper limit of |min. Dst| of 2500 nT and showed that this E_{yp} is possible according to the past observations.
5. Using the CCDF, we estimated the probabilities of E_y of 100, 200, 250, and 340 mV/m occurring over the

next 100 years will be 0.563, 0.110, 0.060, and 0.026, respectively. We also showed the probability of large B_s is small comparing with that of large B because the probability that IMF will turn completely to the south is very low.

The above results suggest that large eruptive flares originating near solar central meridian appear to be an almost necessary condition for a magnetic storm with Dst < − 200 nT. The estimated values of E_y for the 13 March 1989 storm and the 1859 Carrington storm were consistent with those in previous studies (Tsurutani et al. 2003; Boteler 2019). The obtained E_y corresponding to the upper limit of |min. Dst| seems to be feasible on the basis of the past observations. The possibility of this value of E_y occurring over the next 100 years was estimated to be 0.060 using the analysis of the CCDF.

Abbreviations

ACE	Advanced composition explorer
CCDF	Complementary cumulative distribution function
CME	Coronal mass ejection
CPCP	Cross polar cap potential
Dst index	Disturbance storm time index
EIT	Extreme ultraviolet imaging telescope
GIC	Geomagnetically induced current
GOES	Geostationary Operational Environment Satellites
GSM coordinate	Geocentric solar magnetic coordinate
ICME	Interplanetary coronal mass ejection
IMF	Interplanetary magnetic field
NCEI	National Centers for Environmental Information
SC	Sudden commencement
SOHO	Solar hemispheric observatory
SWICS	Solar wind ion composition spectrometer
SXR class	Soft X-ray class
SYM-H	Symmetric disturbance field in H
WDC	World data center

Author contributions
SW analyzed the data and prepared the manuscript. AN and YE provided the impetus for this analysis and made comments on the manuscript. All authors read and approved the final manuscript.

Availability of data and materials
The Dst index was obtained from the WDC for Geomagnetism, Kyoto (http://wdc.kugi.kyoto-u.ac.jp/wdc/Sec3.html). The report of geomagnetic storms was provided by the Kakioka Magnetic Observatory (http://www.kakioka-jma.go.jp/en/index.html). The solar events associated with the geomagnetic storms were investigated using the SOHO LASCO CME catalog (https://cdaw.

Watari *et al. Earth, Planets and Space*   (2023) 75:90

Page 14 of 15

gsfc.nasa.gov/CME_list/index.html) and the GOES flare reports archived in the National Centers for Environmental Information (NCEI), NOAA (https://ngdc.noaa.gov/ngdc.html). Solar wind parameters were analyzed using hourly averaged OMNI data (https://spdf.gsfc.nasa.gov/pub/data/omni/low_res_omni/) and the ACE/SWICS data (https://spdf.gsfc.nasa.gov/pub/data/ace/swics/) from the NASA Space Science Data Coordinated Archive (NSSDCA).

Declarations

Author details
[1]National Institute of Information and Communications Technology, Nukui-Kitamachi 4-2-1, Koganei, Tokyo 184-8795, Japan. [2]Research Institute for Sustainable Humanosphere, Kyoto University, Kyoto, Japan.

References

Araki T (2014) Historically largest geomagnetic sudden commencement (SC) since 1868. Earth Planets Space 66:164. https://doi.org/10.1186/s40623-014-0164-0

Araki T, Takeuchi T, Araki Y (2004) Rise time of geomagnetic sudden commencements—statistical analysis of ground geomagnetic data. Earth Planets Space 56(2):289–293

Baker DN, Li X, Pulkkinen A, Ngwira CM, Mays ML, Galvin AB, Simunac DC (2013) A major solar eruptive event in July 2012: Defining extreme space weather scenarios. Space Weather 11:585–591. https://doi.org/10.1002/swe.20097

Bolduc L (2002) GIC observations and studies in the hydro-quebec power system. J Atmos Solar-Terr Phys 64:1793–1802

Boteler DH (2019) A 21st century view of the March 1989 magnetic storm. Space Weather 17(10):1427–1441. https://doi.org/10.1029/2019SW002278

Burton RK, McPherron R (1975) An empirical relationship between interplanetary conditions and Dst. J Geophys Res 80(31):4202

Cannon PS et al (2013) Extreme space weather: Impacts on engineering systems. Royal Academy of Engineering, London

Carrington RC (1859) Description of a singular appearance seen in the sun on September 1, 1859. Mon Not Roy Astron Soc 20:13–15

Cliver EW, Dietrich WF (2013) The 1859 space weather event revisited: limits of extreme activity. J Space Weather Space Clim 3:A31. https://doi.org/10.1051/swsc/2013053

Cliver EW, Svalgaard L (2004) The 1859 solar terrestrial disturbance and the current limits of extreme space weather activity. Solar Phys 224:407–422

Cliver EW, Feynman J, Garrett HB (1990) An estimate of the maximum speed of the solar wind, 1938–1989. J Geophys Res 95(A10):17103–17112. https://doi.org/10.1029/JA095!A10p17103

Cliver EW, Potzi W, Veronig AM (2022) Large sunspot groups and great magnetic storms: magnetic suppression of CMEs. Astrophys J 938:136. https://doi.org/10.3847/1538-4357/ac847d

Committee on the social and economic impacts of severe space weather events (2008) Severe space weather events–understanding social and economic impacts: a workshop report. National Academies Press, Washington

Ebihara Y, Ejiri M (2003) Numerical simulation of the ring current: review. Space Sci Rev 105:377–452. https://doi.org/10.1023/A:1023905607888

Echer E, Gonzalez WD, Tsurutani BT (2008a) Interplanetary conditions leading to superintense geomagnetic storms (Dst < −250 nT) during solar cycle 23. Geophys Res Lett 35:L06S03. https://doi.org/10.1029/2007GL031755

Echer E, Gonzalez WD, Tsurutani BT, Gonzalez ALC (2008b) Interplanetary conditions causing intense geomagnetic storms (Dst < −100 nT) during solar cycle 23 (1996–2006). J Geophys Res 113:A05221. https://doi.org/10.1029/2007JA012744

Echer E, Tsurutani BT, Gonzalez WD (2013) Interplanetary origins of moderate (−100 nT < Dst ≤ −50 nT) geomagnetic storms during solar cycle 23 (1996–2008). J Geophys Res 118:385–392. https://doi.org/10.1029/2012JA018086

Farrugia CJ, Berdichevsky DB (2004) Evolutionary signatures in complex ejecta and their driven shocks. Ann Geophys 22:3679–3698

Gonzalez WD, Echer E (2005) A study on the peak Dst and peak negative Bz relationship during intense geomagnetic storms. Geophys Res Lett 32:L18103. https://doi.org/10.1029/2005GL023486

Gonzalez WD, Tsurutani BT (1987) Criteria of interplanetary parameters causing intense magnetic storms (Dst < −100 nT). Planet Space Sci 35(9):1101–1109

Gonzalez WD, Gonzalez ALC, Dal Lago A, Tsurutani BT, Arballo JK, Lakhina GS, Buti B, Ho CM, Wu ST (1998) Magnetic cloud field intensities and solar wind velocities. Geophys Res Lett 25:963. https://doi.org/10.1029/98GL00703

Hayakawa H, Nevanlinna H, Blake SP, Ebihara Y, Bhaskar AT, Miyoshi Y (2022) Temporal variations of the three geomagnetic field components at Colaba observatory around the Carrington storm in 1859. ApJ 928:32. https://doi.org/10.3847/1538-4357/ac2601

Iyemori T (1990) Storm-time magnetospheric currents inferred from mid-latitude geomagnetic field variations. J Geomag Geoelectr 42:1249–1265

World Data Center (WDC) for Geomagnetism, Kyoto (2015) Geomagnetic Dst index. https://doi.org/10.17593/14515-74000

Iyemori T, Takeda M, Nose M, Odagiri Y, Toh H (2010) Mid-latitude geomagnetic indices "ASY" and "SYM" for 2009 (provisional). https://wdc_kugi.kyoto-u.ac.jp/aeasy/asy.pdf. Accessed 28 Jan 2023

Kakioka Magnetic Observatory (2015) Kakioka geomagnetic storm catalog 1996–2021. Kakioka Magn Obs Digit Data Serv. https://doi.org/10.48682/386bd.007b0

Kataoka R (2013) Probability of occurrence of extreme magnetic storms. Space Weather 11:214–218. https://doi.org/10.1002/swe.20044

Knipp DJ, Fraser BJ, Shea MA, Smart DF (2018) On the little-known consequences of the 4 August 1972 ultra-fast coronal mass ejecta: facts, commentary, and call to action. Space Weather 16:1635–1643. https://doi.org/10.1029/2018SW002024

Knipp DJ, Bernstein V, Wahl K, Hayakawa H (2021) Timelines as a tool for learning about space weather storms. J Space Weather Space Clim 11:29. https://doi.org/10.1051/swsc/2021011

Kurihara K (2001) Data science in Japanese. NHK Publishing Inc, Tokyo, pp 85–113

Lefevre L, Vennerstrom DM, Vrsnak B, Sudar D, Arlt R, Clette F, Crosby N (2016) Detailed analysis of solar data related to historical extreme geomagnetic storms: 1868–2010. Sol Phys 291:1483–1531. https://doi.org/10.1007/s11207-016-0892-3

Liu YD, Luhmann JG, Kajdic P, Kilpua KJ, Lugaz N, Nitta NV, Mostl C, Lavrud B, Bale SD, Farrugia CJ, Galvin AB (2014) Observations of an extreme storm in interplanetary space caused by successive coronal mass ejections. Nat Commun 5:3481. https://doi.org/10.1038/ncomms4481

Lopez RE, Lyon JG, Mitchell E, Bruntz R, Merkin VG, Brogl S, Toffoletto F, Wiltberger M (2009) Why doesn't the ring current injection rate saturate? J Geophys Res 114:A02204. https://doi.org/10.1029/2008JA013141

Love JJ (2012) Credible occurrence probabilities for extreme geophysical events: Earthquakes, volcanic eruption, magnetic storms. Geophys Res Lett 39:L10301. https://doi.org/10.1029/2012GL051431

Meng X, Tsurutani BT, Mannucci AJ (2019) The solar and interplanetary causes of superstorms (Minimum Dst ≤ −250 nT) during the space ages. J Geophys Res 124:3926–3948. https://doi.org/10.1029/2018JA026425

Myllys M, Kilpua EKJ, Lavraud B, Pulkkinen TI (2016) Solar wind-magnetosphere coupling efficiency during ejects and sheath-driven geomagnetic storms. J Geophys Res 121:4378–4396. https://doi.org/10.1002/2016JA022407

O'Breien TP, McPherron RL (2000) An empirical phase space analysis of ring current dynamics: solar wind control of injection and decay. J Geophys Res 105(A4):7707–7719

Rawat R, Echer E, Gonzalez WD (2018) How different are the solar wind-interplanetary conditions and the consequent geomagnetic activity during the ascending and early descending phases of the solar cycles 23 and

24? J Geophys Res 123:6621–6638. https://doi.org/10.1029/2018JA025683

Reiff PH, Spiro RW, Hill TW (1981) Dependence of polar cap potential drop on interplanetary parameters. J Geophys Res 86(A9):7639–7648

PH Reiff JG Luhmann (1986) Solar wind control of the polar-cap voltage Y Kamide JA Slavin Eds. Solar wind magnetosphere coupling Terr Sci Tokyo

Richardson IG, Webb DF, Zhang J, Berdichevsky DB, Biesecker DA, Kasper JC, Kataoka R, Steinberg JT, Thompson BJ, Wu C-C, Zhukov AN (2006) Major geomagnetic storms (Dst ≤ −100 nT) generated by corotating interaction regions. J Geophys Res 111:A07S09. https://doi.org/10.1029/2005JA011476

Riley P (2012) On the probability of occurrence of extreme space weather events. Space Weather 10(2):S02012. https://doi.org/10.1029/2011SW000734

Russell CT, Luhmann JG, Lu G (2001) Nonlinear response of the polar ionosphere to large values of the interplanetary electric field. J Geophys Res 106(A9):18495–18504. https://doi.org/10.1029/2001JA900053

Russell CT, Mewaldt RA, Luhmann JG, Mason GM, von Rosenvinge TT, Cohen CMS, Leske RA, Gomez-Herrero KA, Galvin AB, Simunac KDC (2013) The very unusual interplanetary coronal mass ejection of 2012 July 23: a blast wave mediated by solar energetic particles. ApJ 770:38. https://doi.org/10.1088/0004-637X/770/1/38

Siscoe G, Crooker NU, Clauer CR (2006) Dst of the carrington storm of 1859. Adv Space Res 38:173–179. https://doi.org/10.1016/j.asr.2005.02.102

Skoug RM, Gosling JT, Steinberg JT, McComas DJ, Smith CW, Ness NF, Hu Q, Burlaga LF (2004) Extremely high speed solar wind: 29–30 October 2003. J Geophys Res 109:A09102. https://doi.org/10.1029/2004JA010494

Sugiura M (1964) Hourly values of equatorial Dst for the IGY. Ann Int Geophys 35:9

Tsubouchi K, Omura Y (2007) Long-term occurrence probabilities of intense geomagnetic storm events. Space Weather 5:S122003. https://doi.org/10.1029/2007SW000329

Tsurutani BT, Gonzalez WD (1997) The interplanetary causes of magnetic storms: a review. In: Tsurutani BT, Gonzalez WD, Kamise Y, Arballo JK (eds) magnetic storms. Geophys Monogr Ser, Washington

Tsurutani BT, Lakhina GS (2014) An extreme coronal mass ejection and consequences for the magnetosphere and Earth. J Geophys Res Lett 41:287–292. https://doi.org/10.1002/2013JGL058825

Tsurutani BT, Gonzalez WD, Lakhina GS, Alex S (2003) The extreme magnetic storm of 1–2 September 1859. J Geophys Res 108(A7):1268. https://doi.org/10.1029/2002JA009504

Vasyliunas VM (2010) The largest imaginable magnetic storm. J Atmos Solar-Terr Phys 73:1444–1446. https://doi.org/10.1016/j.jastp.2010.05.012

Vennerstorm S, Lefevre L, Dumbovic M, Crosby N, Malandraki O, Patsou I, Clette F, Veronig A, Vrsnak B, Leer K, Moretto T (2016) Extreme geomagnetic storms—1868–2010. Sol Phys 291:1447–1481. https://doi.org/10.1007/s11207-016-0897-7-y

von Steiger R, Schwadron NA, Fisk LA, Geiss J, Gloeckler G, Hefti S, Wilken B, Wimmer-Schweingruber RF, Zurbuchen TH (2000) Composition of quasi-stationary solar wind flows from ulysees/solar wind ion composition spectrometer. J Geophys Res 105(A12):27217–27238

Watari S, Kunitake M, Watanabe T (2001) The bastille day (14 July 2000) event in historical large sun-earth connection events. Sol Phys 204:423–436

Wimer DR, Reinleitner LA, Kan JR, Zhu L, Akasofu SI (1990) Saturation of the auroral electrojet current and the polar cap potential. J Geophys Res 95(A11):18981–18987

World Data Center (WDC) for Geomagnetism, Kyoto (2022) Version definitions of AE and Dst geomagnetic indices. https://wdc.kugi.kyoto-u.ac.jp/wdc/pdf/AEDst_version_def_v2.pdf. Accessed 28 Jan 2023

Zhang J, Richardson JG, Webb DF, Gopalswamy N, Huttunen E, Kasper JC, Nitta NV, Poomvises W, Thompson BJ, Wu C-C, Yashiro S (2007a) Solar and interplanetary sources of major geomagnetic storms (≤−100 nT) during 1996–2005. J Geophys Res 112:A10102. https://doi.org/10.1029/2007JA012321

Zhang J, Richardson JG, Webb DF, Gopalswamy N, Huttunen E, Kasper JC, Nitta NV, Poomvises W, Thompson BJ, Wu C-C, Yashiro S (2007b) Correction to "Solar and interplanetary sources of major geomagnetic storms (≤−100 nT) during 1996–2005." J Geophys Res 112:A10103. https://doi.org/10.1029/2007JA012891

Zurbuchen TH, Gloeckler G, Ipavich F, Smith CW, Fisk LA (2004) On the fast coronal mass ejections in October/November 2003: ACE-SWICS results. Geophys Res Lett 31:L11805. https://doi.org/10.1029/2004GL019461

Publisher's Note